Biochemical and mechanical environment cooperatively regulate skeletal muscle regeneration

Sarah Calve[1] and Hans-Georg Simon[2]

Department of Pediatrics, Northwestern University, Feinberg School of Medicine, Children's Memorial Research Center, Chicago, Illinois, USA

ABSTRACT **During forelimb regeneration in the newt *Notophthalmus viridescens*, the dynamic expression of a transitional matrix rich in hyaluronic acid, tenascin-C, and fibronectin controls muscle cell behavior *in vivo* and *in vitro*. However, the influence of extracellular matrix (ECM) remodeling on tissue stiffness and the cellular response to mechanical variations during regeneration was unknown. By measuring the transverse stiffness of tissues *in situ*, we found undifferentiated regenerative blastemas were less stiff than differentiated stump muscle (13.3±1.6 *vs.* 16.6±1.2 kPa). To directly determine how ECM and stiffness combine to affect skeletal muscle fragmentation, migration, and fusion, we coated silicone-based substrates ranging from 2 to 100 kPa with matrices representative of transitional (tenascin-C and fibronectin) and differentiated environments (laminin and Matrigel). Using live-cell imaging, we found softer tenascin-C-coated substrates significantly enhanced migration and fragmentation of primary newt muscle cells. In contrast, stiffer substrates coated with laminin, Matrigel, or fibronectin increased differentiation while suppressing migration and fragmentation. These data support our *in vivo* observations that a transitional matrix of reduced stiffness regulates muscle plasticity and progenitor cell recruitment into the regenerative blastema. These new findings will enable the determination of how biochemical and mechanical cues from the ECM control genetic pathways that drive regeneration.—Calve, S., Simon, H.-G. Biochemical and mechanical environment cooperatively regulate skeletal muscle regeneration. *FASEB J.* 26, 2538–2545 (2012). www.fasebj.org**

Key Words: extracellular matrix · polydimethylsiloxane · live cell imaging · newt · tenascin-C

Appendage regeneration in newts is characterized by an immediate and dramatic remodeling of all tissues proximal to the site of tissue loss. Within the first week after amputation, the collagen and laminin-based extracellular matrix (ECM) that predominates in differentiated, homeostatic tissue is replaced with a transitional ECM rich in fibronectin (FN), hyaluronic acid (HA), and tenascin-C (TN) (1–4). Embedded in this transitional matrix, stem-like progenitor cells are activated and over the following 2 weeks form a regeneration blastema that subsequently restores the lost structure. While the source of blastema cells and the relative contribution of skeletal muscle have been the focus of several studies (5–7), the mechanisms by which progenitor cells are recruited from the stump remain unclear.

Recent work from our laboratory has demonstrated that distinct ECM components can control muscle cell proliferation, migration, fragmentation, and fusion, providing new insights into the instructive function of the changing matrix environment in progenitor cell recruitment and blastema growth (4). The ECM can differentially control cellular behavior through specific binding of matrices to cell membrane localized receptors (*e.g.*, integrins) and mediation of growth factor availability (8, 9). An additional variable linked to the ECM is how composition affects the material properties of biological tissues. A critical role of the ECM is to contribute to tissue structural integrity, and the significant remodeling of the macromolecular composition of the regenerating limb likely alters the local stiffness. Therefore, the deposition of a mechanically different transitional matrix during the early stages of regeneration alters both the biological and mechanical environment, and we hypothesize that these two properties cooperatively influence the recruitment of muscle progenitor cells into the blastema.

Indeed, recent studies have illustrated how subtle changes in stiffness can influence cellular behavior and differentiation (10) and attempts have been made to create physiologically relevant systems *in vitro* to determine the regulatory pathways underlying skeletal muscle behavior (11–16). However, these previous studies considered ECM composition and stiffness as independent and invariant factors, whereas *in vivo* these two properties are intimately intertwined. Here we show for the first time

Abbreviations: dpa, days postamputation; DM, differentiation medium; ECM, extracellular matrix; FN, fibronectin; GM, growth medium; HA, hyaluronic acid; L_p, persistence length; MMP, matrix metalloproteinase; PDMS, polydimethylsiloxane; TN, tenascin-C

[1] Current address: Orthopaedic Research Laboratories, University of Michigan, 109 Zina Pitcher Pl., BSRB 2158, Ann Arbor, MI 48109, USA.

[2] Correspondence: Northwestern University, The Feinberg School of Medicine, Children's Memorial Research Center (CMRC), 2300 Children's Plaza M/C 204, Chicago, IL 60614, USA. E-mail: hgsimon@northwestern.edu

doi: 10.1096/fj.11-200162

how changes in both ECM composition and substrate stiffness combine to control skeletal muscle regeneration.

MATERIALS AND METHODS

Immunohistochemistry

Adult red spotted newts (*Notophthalmus viridescens*) were provided by either Charles Sullivan Company (Nashville, TN, USA) or Connecticut Valley Biological Supply Company (Southampton, MA, USA). Before surgery, newts were anesthetized with 0.1% ethyl 3-aminobenzoate methanesulfonate salt (Sigma, St. Louis, MO, USA) in 0.04% Instant Ocean (Aquarium Systems, Blacksburg, VA, USA). Forelimbs were amputated proximal to the elbow, and animals recovered in 0.25% sulfamerazine sodium salt (Sigma) in 0.04% Instant Ocean. Newts were reanesthetized before regenerating limbs were harvested for immunohistochemistry, as described previously (4). Briefly, 16-μm-thick cryosections were collected, fixed in 4% paraformaldehyde (Sigma) for 5 min, rinsed in PBS (Fisher, Pittsburgh, PA, USA), permeabilized with 0.1% Triton X-100 (Amersham Life Science, Arlington Heights, IL, USA) in PBS for 1 min, and then rinsed with PBS. Sections were blocked for 30 min [blocking buffer: 20% goat serum (Invitrogen, Carlsbad, CA, USA), 0.2% BSA (Sigma), 50 mM ammonium chloride (Sigma), 25 mM glycine (Fisher), 25 mM lysine (Sigma), and 0.02% sodium azide (Sigma) in PBS]. Primary antibodies against TN (1:400, AB19013; Millipore, Billerica, MA, USA) and myosin heavy chain [1:2000; Developmental Studies Hybridoma Bank (DSHB), Iowa City, IA, USA; MF20 ascites] were applied for 1 h, and sections were rinsed with PBS. Slides were blocked again for 5 min before being stained with AF488 anti-rabbit (Invitrogen, Carlsbad, CA, USA), AF546 anti-mouse (Invitrogen), and DAPI (to identify nuclei; Roche, Mannheim, Germany) for 30 min and then were rinsed with PBS and mounted with Fluoro-Gel (Electron Microscopy Sciences, Hatfield, PA, USA).

For thick-section confocal microscopy, we utilized our previously established method (17). Regenerating forelimbs, at 7 days postamputation (dpa), were cryosectioned at 50 μm, fixed in 4% PFA for 10 min, permeabilized with 0.5% Triton X-100 for 30 min, and incubated in blocking buffer for 30 min. Sections were incubated for 24 h at 4°C in 10% goat serum and 0.2% BSA in PBS with the following primary detection agents: mouse anti-chick Pax7 IgG1 (1:800; DSHB); mouse anti-human laminin IgG2a (1:800, 2E8; DSHB); mouse anti-human FN IgG1 (1:300, F0791, Sigma); rabbit anti-chick TN (1:300); biotinylated HA binding protein (1:300, 385911; Calbiochem, La Jolla, CA, USA). Slides were rinsed with PBS 3 × 10 min and placed in blocking buffer for 5–10 min before staining with the following secondary detection reagents for 24 h at 4°C: AF488 anti-mouse IgG (Invitrogen), AF546 streptavidin (Invitrogen), AF546 IgG1 (Invitrogen), DyLight 649 anti-rabbit (Pierce, Rockford, IL, USA), and DAPI (1:1000, Roche). Confocal microscopy was performed on a Zeiss LSM 510 META equipped with 405, Argon/2, HeNe1, and HeNe2 lasers (Carl Zeiss, Thornwood, NY, USA). Confocal *z*-stacks were processed using both ZEN (Carl Zeiss) and Image-Pro Plus 3D constructor (MediaCybernetics, Bethesda, MD, USA).

Mechanical characterization of newt forelimbs

The transverse stiffness of newt tissues was determined *in situ* as described previously (18). Once mid- to late-stage blastemas formed (~3 wk postamputation), newts were anesthetized, and the skin along the dorsal forelimb was carefully removed, taking care to keep the specimens hydrated. The material properties of the muscle that runs along the dorsal side of the humerus (anconeus humeralis lateralis), and the adjacent blastema were determined, measuring the force generated by the controlled displacement of a cylindrical punch (radius 0.19 mm). Since the thickness of the tissues was significantly larger than the punch radius, the following equations could be used to calculate average stress and average strain (19).

$$\sigma = \frac{P}{\pi r^2}$$

$$\varepsilon = \frac{\delta}{r}$$

where P = force, r = radius, and δ = displacement.

Measurements of each tissue were performed in triplicate, and the initial modulus was calculated at ε = 0.5 (n=8 forelimbs).

Generation of substrates of physiologically relevant stiffness

Multiwell polystyrene dishes (24- or 48-wells; Greiner BioOne, Monroe, NC, USA) were coated with Sylgard 527 (Dow Corning, Midland, MI, USA), a dielectric gel composed of polydimethylsiloxane (PDMS), or silicone. Substrates of physiologically relevant stiffness ranging from 2 to 100 kPa were created by varying the ratio of the 2 components of Sylgard 527, A and B, based on the following equation (18):

$$y = 136.7 \exp\left[-2.72\left(\frac{A}{B}\right)\right]$$

where y = desired stiffness (kPa).

After coating with a 1-mm-thick PDMS layer, dishes were left uncovered overnight to offgas, then covered and left undisturbed for ≥2 wk to cure at room temperature. Before functionalizing with different matrix components, PDMS-coated dishes were sterilized with 70% ethanol, rinsed with PBS, and left to dry in a laminar flow cabinet. Individual wells were coated by passive adsorption with TN (2 μg/cm^2; Millipore CC065), FN (2 μg/cm^2; Millipore FC010), laminin (2 μg/cm^2; Millipore CC095), or growth factor reduced Matrigel (100 μg/ml; BD Biosciences, Bedford, MA, USA) diluted in serum-free newt MEM [0.8× MEM (10370, Invitrogen) and 1× Pen/Strep/Fungizone (Fisher)], at 25°C, 2% CO_2. After ≥1 h incubation, ECM solutions were aspirated off, and the dishes were gently rinsed with PBS to remove excess ECM and kept hydrated until plated with cells.

Cell culture

Primary cultures of newt myoblasts were generated from myofiber cultures using previously described methods (4, 20). Mononucleate progenitor cells were expanded under subconfluent conditions in a high-serum growth medium [GM; 0.8× MEM, 10% FBS (SV30014.03; Fisher), 2 mM L-glutamine (Fisher), 1× Pen/Strep/Fungizone, and 25 mM insulin (Sigma)] at 25°C, 2.0% CO_2.

In vitro cell migration assay

Subconfluent myoblasts were trypsinized (0.25% trypsin; Fisher), resuspended in GM, and plated onto PDMS-ECM-coated multiwell plates at 2.5 × 10^3 cells/cm^2. Cells were imaged at 25°C, 2% CO_2 every hour for 24 h using a Leica DMI6000 microscope equipped with an environmental chamber. The total travel distance of cells was determined by manually tracking individual cells using Image-Pro Analyzer (MediaCybernetics). The migration assay was repeated in

quadruplicate using 4 independently isolated primary newt myoblast cell lines. The overall influence of various PDMS-ECM combinations on cell migration was consistent; however, the magnitude in total distance traveled varied between experiments. Therefore, each data set was normalized to the average distance traveled on 100-kPa PDMS before being pooled (n=130 cells for each matrix-stiffness combination).

In vitro myotube fragmentation/fusion assay

Primary newt myoblasts were cultured to confluence in GM and induced to fuse into multinucleate myotubes by switching to low-serum differentiation medium [DM; 0.8×, 1% FBS, 0.4 mM L-glutamine, 1× Pen/Strep/Fungizone, and 2.5 mM insulin]. After incubation in DM for ~1 wk, myotubes were trypsinized, filtered through a 40-μm mesh to remove mononucleate cells, reconstituted in GM, and plated at low density on PDMS-ECM-coated wells. Myotubes were imaged at 25°C, 2% CO_2 every hour for 136 h. Positive fragmentation events were defined as the generation of a cellular fragment from a multinucleate myotube that visibly contained nuclei and was viable for at least 5 h. Percentage fusion was calculated by scoring the number of cells that visibly fused, *via* evidence of cytoplasmic mixing, and then dividing by the total number of myotubes.

Statistical analyses

Two-way ANOVA and Bonferroni's *post hoc* test were used to assess the effects of PDMS stiffness and ECM coating on myoblast migration using Prism (GraphPad Software, La Jolla, CA, USA).

RESULTS

Limb amputation in newts induces dramatic changes in the organization of the ECM surrounding skeletal muscle (**Fig. 1**). In the musculoskeletal system of the normal forelimb, at 0 dpa, the transitional matrix component TN (green) was restricted to the tendons, myotendinous junctions, and periosteum (Fig. 1*A*). By 7 dpa, we detected TN underneath the wound epithelium and at the distal-most end of the retracted skeletal muscle (red, Fig. 1*B*). At the early bud stage (~3 wk postamputation), TN surrounded skeletal muscle myofibers and was expressed throughout the regenerating limb blastema, composed of progenitor cells recruited from the stump tissue (Fig. 1*C*, *D*). On tissue redifferentiation and return to homeostasis, TN became down-regulated in areas of new muscle formation and stayed restricted to the myotendinous junctions and periosteum (Fig. 1*E*, *F*).

To assess the spatial distribution of the transitional matrix in context with individual cells at higher resolution, we imaged 50-μm-thick sections of 7-dpa regenerating forelimbs utilizing a technique previously developed in our laboratory (17). In the intact musculature, HA (red) and FN (data not shown) were restricted to the interstitial space between myofibers (outlined by laminin in white, **Fig. 2*A***). TN (green) was exclusively detected at the myotendinous junctions on the extracellular side of the basal lamina (Fig. 2*A*). Satellite cells were tightly surrounded by the laminin-rich basal lamina (arrowheads, Fig. 2*A*, *B*). In contrast, within areas where regenerative processes have been activated, we could demonstrate a significant enrichment of HA, TN, and FN in the interstitial space (Fig. 2*C*, *F*). While the up-regulation of FN within the basal laminar space was less dramatic, the expression of this HA, TN, and FN-rich transitional matrix extended across the basal lamina and could be detected at the satellite cell-myofiber interface (arrowheads, Fig. 2*C*–*F*). To confirm the spatial identity of satellite cells, sections were stained with Pax7, a transcription factor expressed in undifferentiated myogenic progenitors (21). Three-dimensional imaging revealed $Pax7^+$ mononuclear cells (red) tightly surrounded by laminin (white) and bound to the adjacent myofiber (arrowheads, Fig. 2*G*, *H*). In damaged muscles close to the amputation plane, TN (green) was highly up-regulated throughout, also infiltrating the basal lamina surrounding $Pax7^+$ satellite cells (arrowheads, Fig. 2*I*, *J*). These data indicate that the transitional matrix directly interacts with myofibers and satellite cells in regenerating tissues.

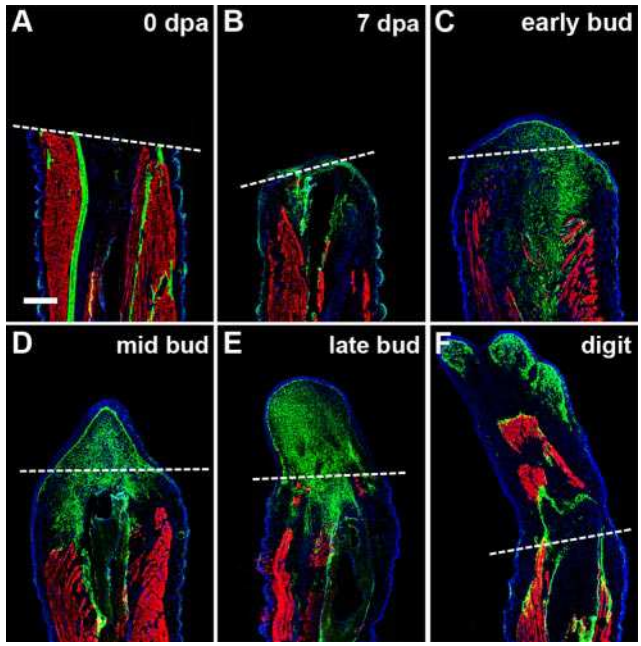

Figure 1. Stump tissue proximal to amputation plane undergoes significant remodeling during limb regeneration. *A*) TN (green), a main component of the transitional matrix up-regulated during regeneration, was only expressed in discrete regions in the normal limb. *B–D*) Soon after amputation, TN expression was enriched within the stump, surrounding the skeletal muscle (MF20, red), and distributed throughout the regenerative blastema that forms distal to the amputation plane (dotted line). *E*, *F*) TN became down-regulated in both the stump and the newly forming limb as the tissues begin to differentiate. Blue indicates DAPI. Scale bar = 400 μm.

To test if ECM reorganization changes the material properties within the regenerating limb, we determined the stiffness of skeletal muscle and the blastema *in situ*. We focused on the anconeus humeralis lateralis (AHL), a large muscle most superficial on the dorsal side of the stylopod (**Fig. 3*A***). Upon amputation proximal to the elbow, the AHL remains largely intact, potentially contributing directly to the blastema that forms immediately distal to this region. Figure 3*B* shows the stress-strain response of the AHL and blastema

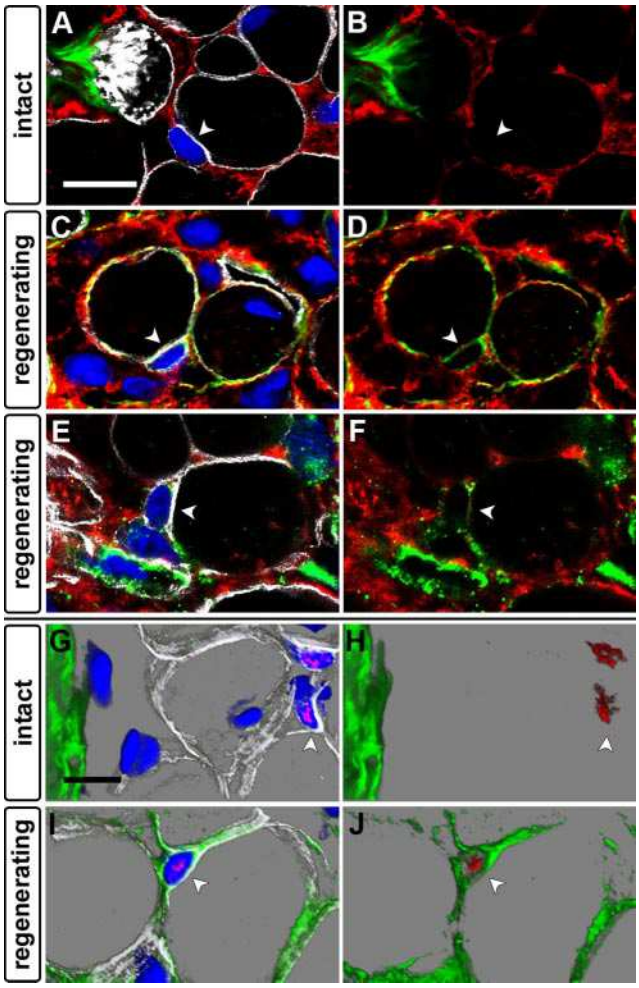

Figure 2. Composition of the local ECM dramatically changes around myofibers proximal to the amputation plane. *A–D*) Confocal images of intact and damaged areas of the same cross-section from a 7-dpa regenerating forelimb. *A*, *B*) Within intact muscle, TN (green) is exclusively detected in the myotendinous junctions (top left) and HA (red) is restricted to the interstitial space. A satellite cell (arrowhead) can be seen on the periphery of a myofiber, separated from the interstitial matrix by the basal lamina (laminin, white). *C*, *D*) Within damaged regions of the regenerating stump, TN and HA were upregulated throughout the enlarged interstitial space and found directly interacting with myofibers and satellite cells. Notably, the transitional matrix has infiltrated the space between the satellite cell and the adjacent myofiber (arrowhead), potentially to facilitate cellular deadhesion and recruitment to the regenerative blastema. *E*, *F*) FN (green) was also expressed around satellite cells in regenerating muscles (arrowhead). *G–J*) Three-dimensional reconstruction reveals how the TN-rich transitional matrix directly interacts with myofibers and satellite cells. *G*, *H*) $Pax7^+$ satellite cells (arrowheads, red) were confined by the laminin-rich basal lamina (white), with TN (green) only expressed in the tendons (left). *I*, *J*) In damaged skeletal muscle, TN infiltrated the basal lamina and fully surrounded the $Pax7^+$ cell (arrowhead). Blue indicates DAPI. View: ×63. Rendered as a 3-dimensional image using Image-Pro Analyzer (MediaCybernetics). Scale bars = 20 μm.

from the same regenerating forelimb, illustrating the consistency of the method and the different material response of these two tissues. The blastema stiffened up around ε = 2, whereas the muscle showed a more gradual stiffening response. However, calculation of the initial moduli of the tissues around a more physiologically relevant strain field (ε=0.5), revealed a reduced stiffness of 13.3 ± 1.6 kPa for the blastema as compared to the previously reported 16.6 ± 1.2 kPa for the adjacent muscle (18), which is a substantial, but not statistically significant, difference (P=0.07; Fig. 3*C*). These results suggest that the deposition of the transitional matrix modulates the local tissue properties and creates a proximodistal stiffness gradient from high in the stump to low in the blastema.

Our testing apparatus only measured the bulk material properties of the forelimb and did not have the resolution to determine the local network stiffness that cells encounter *in vivo*. To directly assess how subtle variations in the mechanical environment may influence muscle cell behavior, we characterized silicone-based PDMS substrates with stiffness tunable in the physiological range. Substrates of 2, 15, 35, and 100 kPa were generated, as described previously (18), to resemble the stiffness of liver, skeletal muscle, arteries, and skin, respectively (10). PDMS was coated with matrices indicative of either the transitional (TN and FN) or differentiated (laminin and Matrigel) extracellular environment. Matrigel is rich in laminin and type IV collagen, components of the basal lamina, and known to enhance muscle differentiation (4). To ensure only a thin layer of ECM was adsorbed onto the PDMS, matrices were diluted to concentrations that did not support gelation, incubated for at least 1 h to allow for passive absorption, and then rinsed to remove excess ECM.

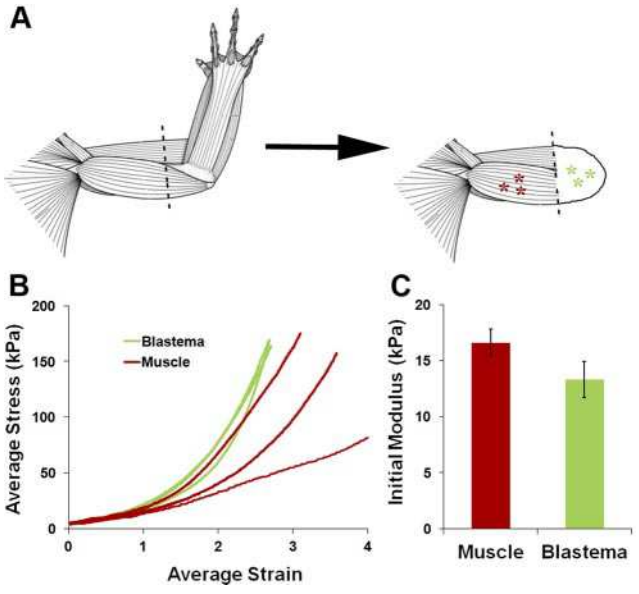

Figure 3. *In situ* indentation testing revealed forelimb skeletal muscle and blastema tissues differ in their material response. *A*) Forelimbs were amputated proximal to the elbow (dotted line). At midbud blastema stage, the stiffness of the anconeus humeralis lateralis and the adjacent regenerating blastema was measured in triplicate (asterisks; schematic adapted from ref. 48). *B*) Stress-strain response of the blastema differed from that of the skeletal muscle, stiffening up at ε = 2. *C*) Measurement of the initial moduli indicated that the undifferentiated blastemas were less stiff (13.3±1.6 kPa) than the differentiated anconeus humeralis lateralis (16.6±1.2 kPa). Error bars = SE; n = 8; P = 0.07.

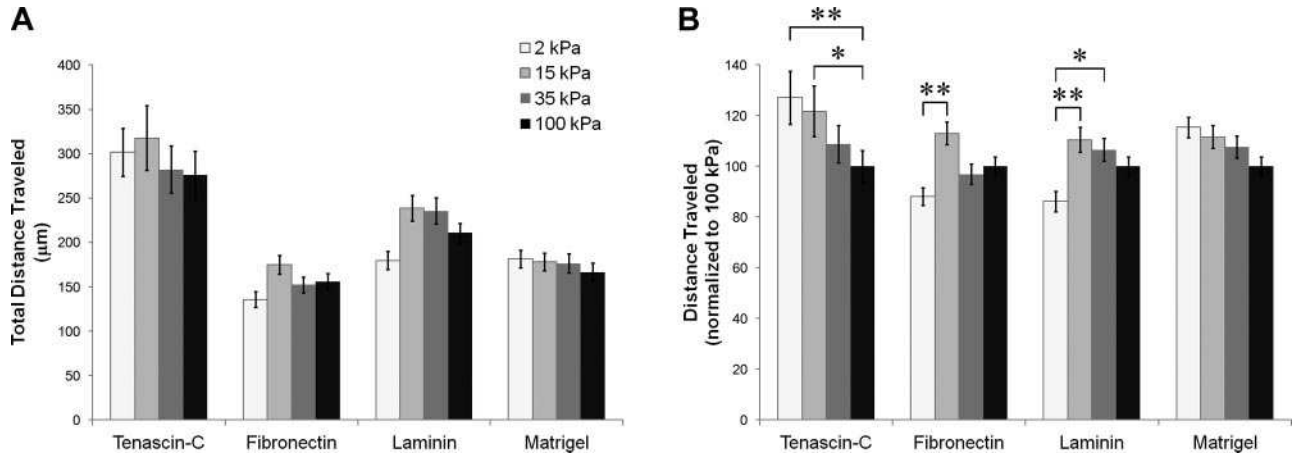

Figure 4. Myoblast migratory response to changes in stiffness is dependent on ECM coating. *A*) Pooled raw data from 4 separate experiments document overall enhancement of myoblast migration on TN and laminin, irrespective of substrate stiffness. Two-way ANOVA revealed a significant influence of ECM coating on migration ($P<0.0001$), and myoblasts traveled significantly farther on TN as compared to all other ECM-stiffness combinations, except laminin-coated 15-kPa PDMS. *B*) Normalized myoblast migration on PDMS coated with TN or Matrigel inversely correlated with increased substrate stiffness. However, cell migration on FN- and laminin-coated PDMS was enhanced on 15-kPa substrates (stiffness similar to newt skeletal muscle; Fig. 3). Two-way ANOVA revealed significance for matrix/stiffness cooperation ($P<0.005$), ECM coating ($P<0.001$), and PDMS stiffness ($P<0.005$). Significance of PDMS stiffness on distance traveled for each ECM coating was calculated using Bonferroni's *post hoc* test. Primary newt myoblasts were imaged for 24 h. Error bars = SE, $n = 130$ cells/PDMS-ECM combination. $^*P < 0.05$; $^{**}P < 0.01$.

Primary newt myoblasts demonstrated differential migratory behavior as a function of substrate stiffness and coating (**Fig. 4**). Regardless of stiffness, myoblasts covered a significantly greater distance in 24 h on TN than on the other ECMs ($P<0.0001$; Fig. 4*A*), consistent with our previous results (4). When the data for each ECM were normalized to 100 kPa to account for overall cell motility differences between the four replicate runs, we found that the distance traveled on TN-coated PDMS decreased significantly as stiffness increased from 2 to 100 kPa ($P<0.01$) with cells on Matrigel following a similar trend (Fig. 4*B*). In contrast, myoblasts plated on FN and laminin migrated the farthest on substrates with a stiffness comparable to muscle. Two-way ANOVA revealed significance for both ECM coating ($P<0.001$) and PDMS stiffness ($P<0.005$). In sum, these results indicate that a TN-rich environment with reduced stiffness enhances myoblast migration.

To investigate whether ECM and stiffness combine to provide integrated cues that control skeletal muscle plasticity, differentiated, multinucleate myotubes were followed using time-lapse microscopy over a 5-day period. When plated on TN-coated 15 kPa PDMS, myotubes preferentially fragmented into viable cells, whereas little to no viable fragmentation occurred on FN, laminin, or Matrigel-coated PDMS (**Fig. 5*A***). In contrast, under the same culture conditions, FN, laminin, and Matrigel enhanced cell fusion (Fig. 5*B*). Of note, FN and laminin substrates of 15-35 kPa induced higher fusion rates overall, whereas 2-kPa

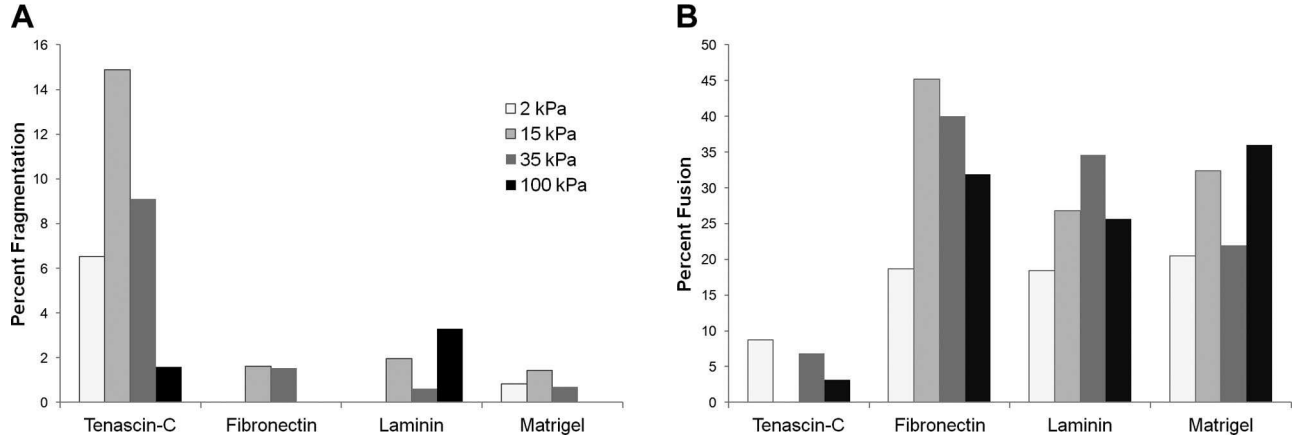

Figure 5. ECM and substrate stiffness combine to control the differentiation state of skeletal muscle cells. *A*) Primary newt myotubes preferentially fragmented into viable cells on PDMS-TN substrates of 15 kPa, whereas little to no fragmentation was supported by the other PDMS-ECM combinations tested. *B*) Under the same culture conditions, myotube fusion was inhibited on PDMS-TN substrates, but was enhanced on FN, laminin and Matrigel, particularly on 15- and 35-kPa PDMS. Myotubes were imaged for 136 h; $n \geq 44$ myotubes/PDMS-ECM combination.

PDMS revealed the lowest fusion potential. These results demonstrate that the ECM composition and substrate stiffness cooperatively control whether myotubes go toward a dedifferentiation (*i.e.*, fragmentation) or differentiation (*i.e.*, fusion) pathway.

DISCUSSION

What sets regeneration apart from tissue formation during embryogenesis is that new structures have to be built in context of preexisting differentiated tissues. Therefore, the highly organized tissues remaining in the stump after amputation undergo significant remodeling to create an environment amenable for regeneration. ECM-degrading matrix metalloproteases (MMPs) have a critical role in the breakdown of the musculoskeletal connective tissues, and experimental inhibition of MMPs results in scar formation at the amputation plane at the expense of regenerative growth (22). During this remodeling process, the collagen-rich matrix typical for differentiated tissues is temporarily replaced by a transitional ECM rich in HA, TN, and FN that, in combination with soluble factors expressed by the wound epithelium, creates an environment largely resembling that of the developing limb, albeit on a larger scale (23).

We previously demonstrated an instructive role of ECM remodeling for progenitor cell recruitment during regeneration, promoting muscle fragmentation, proliferation, and migration (4, 17). Here we hypothesized that progenitor cell recruitment will also be influenced by variations in the mechanical environment due to changes in the structural organization of regenerating tissue. By measuring the transverse stiffness of a midbud regenerating limb, we indeed found the regenerating blastema to be less stiff than muscle in the stump, suggesting that the infiltrating matrix generates a gradient in material properties along the proximal-distal axis (Figs. 1 and 3).

Our data for the transverse stiffness of skeletal muscle (15–61 kPa) are in line with published values (24–27); however, the difference between blastema and muscle did not meet statistical significance. This may be attributed to the punch radius of our indenter being much larger than individual cells and unable to resolve the mechanical properties of individual tissue components. The mechanical properties of native ECM networks, on the scale at which cells sense the local environment, have only been characterized for a few systems, but it is clear that the pericellular matrix does not necessarily have the same material response as the bulk tissue (28–30). Therefore, when the macromolecular architectural differences between differentiated muscle and undifferentiated regenerative blastema are taken into account, there is likely a greater difference in the stiffness cells encounter than what we could experimentally determine.

The ECM surrounding individual myofibers is highly organized, composed of a mesh-like basal lamina of laminin and cross-linked type IV collagen that is structurally more rigid than the myofiber it envelops (31–33). An external network of type I and III collagen fibrils are connected to the basal lamina, facilitating the transfer of muscle-generated force through tendon to bone (34). The tightly packed myofibers are embedded in an interstitial network of HA, FN, and various proteoglycans (35, 36).

In contrast, the ECM of the regenerating limb is more loosely packed. There is considerable edema proximal to the amputation plane, lowering the cellular density as compared to intact differentiated tissues (37). The increase in hydration and decrease in density are most likely due to the up-regulation of HA (Fig. 2), an anionic linear glycosaminoglycan with a large hydrodynamic volume (38, 39). TN, a large hexameric glycoprotein typically restricted to areas of high mechanical loading such as tendons and myotendinous junctions (40), was also substantially up-regulated within regenerating muscle (Figs. 1 and 2). In injured muscle, TN up-regulation is thought to play a role in decreasing cellular adhesion to prevent further injury (41). These disparate functions may be partially attributed to the significant extensibility and flexibility of the TN molecule. Molecular flexibility can be characterized by fitting experimental force-displacement data with the worm-like chain model (42), which results in persistence length (L_p) values of 0.42 nm and 4.5 nm for TN and HA, respectively, where a larger L_p correlates with a stiffer chain (43, 44). Notably, $L_p > 14$ nm for the type I collagen triple helix indicates that at the molecular level this component of the differentiated matrix is inherently stiffer than TN and HA (45). Considering the micromechanical data presented above, it is apparent that during regeneration, the ECM surrounding skeletal muscle proximal to the amputation site shifts from a highly ordered and rigid microenvironment to a loosely packed and flexible transitional ECM of reduced stiffness.

To decipher how the transitional matrix promotes progenitor cell recruitment, we developed an *in vitro* culture system that allows for the modulation of both stiffness and matrix composition using physiologically relevant PDMS-ECM combinations. This system enabled the simulation of biological processes outside the complex *in vivo* environment. For example: $Pax7^+$ satellite cells within an uninjured muscle are surrounded by a rigid basal lamina. If erroneously activated, our data indicate that the stiff collagen- and laminin-rich ECM will provide an effective negative feedback mechanism to limit satellite cell migration and rapidly induce fusion (**Fig. 6**). In a muscle with localized injury, such as generated during exercise-induced overloading, the basal lamina is partially disrupted and satellite cells are exposed to ECM typically restricted to the interstitial space. Stimulated by the local change in ECM composition, myoblasts will rapidly migrate along the FN- and laminin-rich myofiber surface (Fig. 4). However, we found that these combinations of matrix type and stiffness also induce fusion, leading to competing behaviors that may prevent activated satellite cells from migrating away from the local site of injury. In contrast, after tissue damage with significant myofiber death, the transitional matrix will infiltrate the muscle tissue completely, resulting in an overall decrease of tissue stiffness (Figs. 1–3). The TN-rich ECM is highly conducive for cell fragmentation and migration while inhibiting fusion, indicating that the softer transitional matrix environment facilitates myoblast recruitment from the stump to the blastema (Figs. 4–6). The expression of FN around satellite cells was unexpected as our *in vitro* data indicated this ECM promotes fusion (Fig. 5); how-

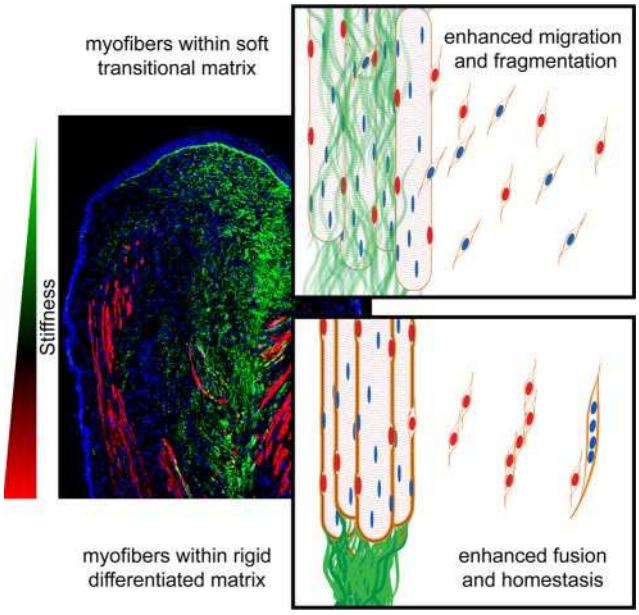

Figure 6. Model of cooperative biochemical and mechanical function of the regenerative transitional matrix on cell behavior. In the regenerating limb, a stiffness gradient is established ranging from the more proximal, differentiated skeletal muscle (red) in the stump to the distal, TN-rich blastema (green). Bottom right: intact myofibers are tightly packed and surrounded by a rigid ECM network (orange). If satellite cells (red nuclei) become activated in this stiff laminin and type IV collagen-rich differentiated environment, they are by default prone to fuse with neighboring muscle cells. Top right: in contrast, myofibers within the distal regions experience a more hydrated and less dense matrix environment. Breakdown of the differentiated ECM enables muscle cells to come into direct contact with the transitional matrix, leading to the recruitment of blastema progenitors from both the $Pax7^+$ satellite cell and myofiber populations.

ever, the coexpression of TN and HA may mask or override the prodifferentiation epitopes of FN. At later stages of regeneration, the down-regulation of TN and HA in areas of muscle differentiation (Fig. 1; ref. 4) may be important to not only eliminate the biochemical inhibition of fusion, but the decrease in hydration will lead to an increase in local stiffness and bring cells in close proximity, ultimately facilitating cell-cell communication and differentiation.

Our observations that a stiff tissue environment promotes muscle homeostasis may provide insight into why gene- and cell-based therapies often fail to alleviate fibrotic diseases in human skeletal muscle (46). Muscular dystrophy and sarcopenia are both characterized by a pathological up-regulation of collagenous matrices that increase the overall stiffness of the muscular ECM (47). The stiffer fibrotic environment will stimulate activated satellite cells to fuse rather than proliferate and migrate, contributing to a positive feedback loop that favors fibrosis over functional muscle restoration (46). Therefore, it will be necessary to develop integrated intervention strategies that allow both the induction of appropriate ECM remodeling and activation of satellite cells to achieve functional repair.

Our data clearly demonstrate that variations in ECM composition and substrate stiffness cooperate to control cell behavior. These findings indicate that standard tissue culture assays, which greatly deviate from the biomechanical properties of most physiological systems, pose a substantial risk that certain cellular mechanisms may be missed. What sets this study apart from related work investigating the combined influence of stiffness and matrix on cell behavior (11–16) is the consideration of the dynamic *in vivo* situation. We characterized the material properties of the regenerating system *in vivo* first, comparing the variations in both ECM composition and stiffness between homeostatic and injured regions. Then we used this information to establish an *in vitro* environment to directly test and demonstrate how the biochemical and mechanical properties of the changing matrix combine to regulate the plasticity of skeletal muscle. With this new knowledge, we can now create physiologically relevant systems that will enable us to determine, under defined conditions, the underpinning regulatory pathways that control the differentiation state of muscle during regenerative processes. FJ

The authors thank Dr. K. Shull and K. Otim (Department of Materials Science and Engineering, Northwestern University) for assistance with mechanical testing. The authors also thank all members of the H.-G.S. laboratory for helpful discussions. The authors are grateful to Dr. C. Huppenbauer and M. Tjepkema (W. Nuhsbaum Inc., McHenry, IL, USA) for expert technical support. This work was supported by the U.S. Defense Advanced Research Projects Agency, Restorative Injury Repair BAA04-12 Addendum B (to H.-G.S.), Searle Funds at The Chicago Community Trust (to H.-G.S.), and the U.S. National Institutes of Health T90 Regenerative Medicine Training Program (to S.C.).

REFERENCES

1. Repesh, L. A., Fitzgerald, T. J., and Furcht, L. T. (1982) Changes in the distribution of fibronectin during limb regeneration in newts using immunocytochemistry. *Differentitation* **22,** 125–131
2. Tassava, R. A., Nace, J. D., and Wei, Y. (1996) Extracellular matrix protein turnover during salamander limb regeneration. *Wound Repair Regen.* **4,** 75–81
3. Toole, B. P., and Gross, J. (1971) The extracellular matrix of the regenerating newt limb: synthesis and removal of hyaluronate prior to differentiation. *Dev. Biol.* **25,** 57–77
4. Calve, S., Odelberg, S. J., and Simon, H. G. (2010) A transitional extracellular matrix instructs cell behavior during muscle regeneration. *Dev. Biol.* **344,** 259–271
5. Morrison, J. I., Loof, S., He, P. P., and Simon, A. (2006) Salamander limb regeneration involves the activation of a multipotent skeletal muscle satellite cell population. *J. Cell Biol.* **172,** 433–440
6. Kumar, A., Velloso, C. P., Imokawa, Y., and Brockes, J. P. (2004) The regenerative plasticity of isolated urodele myofibers and its dependence on *Msx1*. PLoS Biol. **2,** 1168–1176
7. Kragl, M., Knapp, D., Nacu, E., Khattak, S., Maden, M., Epperlein, H. H., and Tanaka, E. M. (2009) Cells keep a memory of their tissue origin during axolotl limb regeneration. *Nature* **460,** 60–69
8. Legate, K. R., Wickstrom, S. A., and Fassler, R. (2009) Genetic and cell biological analysis of integrin outside-in signaling. *Genes Dev.* **23,** 397–418
9. Schultz, G. S., and Wysocki, A. (2009) Interactions between extracellular matrix and growth factors in wound healing. *Wound Repair Regen.* **17,** 153–162
10. Nemir, S., and West, J. L. (2010) Synthetic materials in the study of cell response to substrate rigidity. *Ann. Biomed. Eng.* **38,** 2–20
11. Engler, A. J., Griffin, M. A., Sen, S., Bonnetnann, C. G., Sweeney, H. L., and Discher, D. E. (2004) Myotubes differentiate optimally

on substrates with tissue-like stiffness: pathological implications for soft or stiff microenvironments. *J. Cell Biol.* **166,** 877–887
12. Boonen, K. J. M., Rosaria-Chak, K. Y., Baaijens, F. P. T., van der Schaft, D. W. J., and Post, M. J. (2009) Essential environmental cues from the satellite cell niche: optimizing proliferation and differentiation. *Am. J. Physiol. Cell Physiol.* **296,** C1338–1345
13. Maley, M. A. L., Davies, M. J., and Grounds, M. D. (1995) Extracellular matrix, growth factors, genetics: Their influence on cell proliferation and myotube formation in primary cultures of adult mouse skeletal muscle. *Exp. Cell Res.* **219,** 169–179
14. Macfelda, K., Kapeller, B., Wilbacher, I., and Losert, U. M. (2007) Behavior of cardiomyocytes and skeletal muscle cells on different extracellular matrix components–relevance for cardiac tissue engineering. *Artif. Organs* **31,** 4–12
15. Gilbert, P. M., Havenstrite, K. L., Magnusson, K. E. G., Sacco, A., Leonardi, N. A., Kraft, P., Nguyen, N. K., Thrun, S., Lutolf, M. P., and Blau, H. M. (2010) Substrate elasticity regulates skeletal muscle stem cell self-renewal in culture. *Science* **329,** 1078–1081
16. Ren, K. F., Fourel, L., Rouviere, C. G., Albiges-Rizo, C., and Picart, C. (2010) Manipulation of the adhesive behaviour of skeletal muscle cells on soft and stiff polyelectrolyte multilayers. *Acta Biomater.* **6,** 4238–4248
17. Calve, S., and Simon, H. G. (2011) High resolution three-dimensional imaging: Evidence for cell cycle reentry in regenerating skeletal muscle. *Dev. Dyn.* **240,** 1233–1239
18. Calve, S., and Simon, H. G. (2010) Extracellular control of limb regeneration. In *IUTAM Symposium on Cellular, Molecular and Tissue Mechanics* (Arruda, E. M., and Garikipati, K., eds) Vol. 16, pp. 257–266, Springer, Dordrecht, The Netherlands
19. Shull, K. R. (2002) Contact mechanics and the adhesion of soft solids. *Mater. Sci. Eng. R. Rep.* **36,** 1–45
20. Kumar, A., and Brockes, J. P. (2007) Preparation of cultured myofibers from larval salamander limbs for cellular plasticity studies. *Nat. Protoc.* **2,** 939–947
21. Seale, P., Sabourin, L. A., Girgis-Gabardo, A., Mansouri, A., Gruss, P., and Rudnicki, M. A. (2000) Pax7 is required for the specification of myogenic satellite cells. *Cell* **102,** 777–786
22. Vinarsky, V., Atkinson, D. L., Stevenson, T. J., Keating, M. T., and Odelberg, S. J. (2005) Normal newt limb regeneration requires matrix metalloproteinase function. *Dev. Biol.* **279,** 86–98
23. Rowe, D. A., and Fallon, J. F. (1982) The proximodistal determination of skeletal parts in the developing chick leg. *J. Embryol. Exp. Morph.* **68,** 1–7
24. Bosboom, E. M. H., Hesselink, M. K. C., Oomens, C. W. J., Bouten, C. V. C., Drost, M. R., and Baaijens, F. P. T. (2001) Passive transverse mechanical properties of skeletal muscle under in vivo compression. *J. Biomech.* **34,** 1365–1368
25. Collinsworth, A. M., Zhang, S., Kraus, W. E., and Truskey, G. A. (2002) Apparent elastic modulus and hysteresis of skeletal muscle cells throughout differentiation. *Am. J. Physiol. Cell Physiol.* **283,** C1219–1227
26. Defranchi, E., Bonaccurso, E., Tedesco, M., Canato, M., Pavan, E., Raiteri, R., and Reggiani, C. (2005) Imaging and elasticity measurements of the sarcolemma of fully differentiated skeletal muscle fibres. *Microsc. Res. Tech.* **67,** 27–35
27. Ogneva, I. V., Lebedev, D. V., and Shenkman, B. S. (2010) Transversal stiffness and Young's modulus of single fibers from rat soleus muscle probed by atomic force microscopy. *Biophys. J.* **98,** 418–424
28. Candiello, J., Balasubramani, M., Schreiber, E. M., Cole, G. J., Mayer, U., Halfter, W., and Lin, H. (2007) Biomechanical properties of native basement membranes. *FEBS J.* **274,** 2897–2908
29. Darling, E. M., Wilusz, R. E., Bolognesi, M. P., Zauscher, S., and Guilak, F. (2010) Spatial mapping of the biomechanical properties of the pericellular matrix of articular cartilage measured in situ via atomic force microscopy. *Biophys. J.* **98,** 2848–2856
30. Han, L., Grodzinsky, A. J., and Ortiz, C. (2011) Nanomechanics of the cartilage extracellular matrix. In *Annual Review of Materials Research* (Clarke, D. R., and Fratzl, P., eds) Vol. 41, pp. 133–168, Annual Reviews, Palo Alto, CA, USA
31. Rowe, R. G., and Weiss, S. J. (2008) Breaching the basement membrane: who, when and how? *Trends Cell Biol.* **18,** 560–574
32. Sanes, J. R. (2003) The basement membrane/basal lamina of skeletal muscle. *J. Biol. Chem.* **278,** 12601–12604
33. Han, R., Kanagawa, M., Yoshida-Moriguchi, T., Rader, E. P., Ng, R. A., Michele, D. E., Muirhead, D. E., Kunz, S., Moore, S. A., Iannaccone, S. T., Miyake, K., McNeil, P. L., Mayer, U., Oldstone, M. B., Faulkner, J. A., and Campbell, K. P. (2009) Basal lamina strengthens cell membrane integrity via the laminin G domain-binding motif of alpha-dystroglycan. *Proc. Natl. Acad. Sci. U. S. A.* **106,** 12573–12579
34. Kjaer, M. (2004) Role of extracellular matrix in adaptation of tendon and skeletal muscle to mechanical loading. *Physiol. Rev.* **84,** 649–698
35. Grounds, M. D. (2008) Complexity of extracellular matrix and skeletal muscle regeneration. In *Skeletal Muscle Repair and Regeneration* (Schiaffino, S., and Partridge, T., eds) Vol. 3, pp. 269–301, Springer, Dordrecht, The Netherlands
36. Okita, M., Yoshimura, T., Nakano, J., Motomura, M., and Eguchi, K. (2004) Effects of reduced joint mobility on sarcomere length, collagen fibril arrangement in the endomysium, and hyaluronan in rat soleus muscle. *J. Muscle Res. Cell Motil.* **25,** 159–166
37. Chalkley, D. T. (1954) A quantitative histological analysis of forelimb regeneration in *Triturus viridescens*. *J. Morphol.* **94,** 21–70
38. Fraser, J. R. E., Laurent, T. C., and Laurent, U. B. G. (1997) Hyaluronan: Its nature, distribution, functions and turnover. *J. Intern. Med.* **242,** 27–33
39. Mescher, A. L., and Cox, C. A. (1988) Hyaluronate accumulation and nerve-dependent growth during regeneration of larval ambystoma limbs. *Differentiation* **38,** 161–168
40. Jarvinen, T. A. H., Jozsa, L., Kannus, P., Jarvinen, T. L. N., Hurme, T., Kvist, M., Pelto-Huikko, M., Kalimo, H., and Jarvinen, M. (2003) Mechanical loading regulates the expression of tenascin-C in the myotendinous junction and tendon but does not induce de novo synthesis in the skeletal muscle. *J. Cell Sci.* **116,** 857–866
41. Mackey, A. L., Brandstetter, S., Schjerling, P., Bojsen-Moller, J., Qvortrup, K., Pedersen, M. M., Doessing, S., Kjaer, M., Magnusson, S. P., and Langberg, H. (2011) Sequenced response of extracellular matrix deadhesion and fibrotic regulators after muscle damage is involved in protection against future injury in human skeletal muscle. *FASEB J.* **25,** 1943–1959
42. Bouchiat, C., Wang, M. D., Allemand, J. F., Strick, T., Block, S. M., and Croquette, V. (1999) Estimating the persistence length of a worm-like chain molecule from force-extension measurements. *Biophys. J.* **76,** 409–413
43. Luo, Z. P., Sun, Y. L., Fujii, T., and An, K. N. (2004) Single molecule mechanical properties of type II collagen and hyaluronan measured by optical tweezers. *Biorheology* **41,** 247–254
44. Oberhauser, A. F., Marszalek, P. E., Erickson, H. P., and Fernandez, J. M. (1998) The molecular elasticity of the extracellular matrix protein tenascin. *Nature* **393,** 181–185
45. Sivakumar, L., and Agarwal, G. (2010) The influence of discoidin domain receptor 2 on the persistence length of collagen type I fibers. *Biomaterials* **31,** 4802–4808
46. Serrano, A. L., Mann, C. J., Vidal, B., Ardite, E., Perdiguero, E., and Munoz-Canoves, P. (2011) Cellular and molecular mechanisms regulating fibrosis in skeletal muscle repair and disease. In *Current Topics in Developmental Biology: Myogenesis* (Pavlath, G. K., ed) Vol. 96, pp. 167–201, Elsevier Academic, San Diego, CA, USA
47. Hakim, C. H., Grange, R. W., and Duan, D. S. (2011) The passive mechanical properties of the extensor digitorum longus muscle are compromised in 2- to 20-mo-old mdx mice. *J. Appl. Physiol.* **110,** 1656–1663
48. Walthall, J. C., and Ashley-Ross, M. A. (2006) Postcranial myology of the California newt, *Taricha torosa*. *Anat. Rec.* **288A,** 46–57

Received for publication November 21, 2011.
Accepted for publication February 21, 2012.